Properties of Poly(Ethylene Terephthalate) Prepared by High-Pressure Extrusion in a Capillary Die

PHILLIP D. GRISWOLD and JOHN A. CUCULO, *Department of Textile Chemistry, North Carolina State University, Raleigh, North Carolina 27607*

Synopsis

The procedure of Southern and Porter has been used to prepare poly(ethylene terephthalate) segments by high-pressure extrusion in an Instron capillary rheometer at temperatures from 245° to 265°C. X-Ray measurements of crystalline orientation along the axis of long-growth segments showed that segment properties were controlled by the time-dependent crystallization of polymer melt in the rheometer reservoir. During the initial stage of extrusion, a highly oriented, translucent segment was generated by flow-induced crystallization. However, formation of the translucent morphology eventually stopped, and thereafter a poorly oriented, opaque segment was generated by solid-state extrusion. From wide- and small-angle x-ray scattering, differential scanning calorimetry, and density measurements, it was determined that the most perfect morphologies were prepared at an extrusion temperature of 265°C. In addition to having the highest degree of crystalline orientation, translucent segments extruded at 265°C have a peak melting point of 267°C and a crystallinity value of 62%. Hot-stage optical microscopy showed that the translucent segments contained axially aligned fibrous crystals whose birefringence persisted to 290°C. The exceptional thermal stability of the segments was corroborated by the results of shrinkage tests at temperatures near the melting point; even after 1 hr at 260°C, the shrinkage did not exceed 7%. The accumulated evidence suggests that the translucent segments contain an extended-chain component.

INTRODUCTION

Research on the formation of high-modulus fibers and films from synthetic polymers has accelerated rapidly since about 1970. Both chemical and physical approaches have been taken by researchers in their attempts to fabricate highly oriented, extended-chain morphologies. Those taking the chemical approach have sought to synthesize new polymers with chain backbones which are predisposed to extended configurations and which may be fabricated by existing procedures. An outstanding example of the chemical approach is the synthesis of para-oriented aromatic polymers, which are fabricated into ultrahigh-modulus fibers by solution spinning and drawing techniques.[1] Those taking the physical approach have sought to synthesize new fabrication procedures which may be used to induce high chain alignment and extension with existing polymers. Many investigators[2–11] have attempted to judiciously integrate the controlled flow of flexible-chain polymers with temperature and pressure in order to prepare fibers, films, and tubes of exceptional stiffness and strength.

Perhaps the most successful combination of flow, temperature, and pressure factors has been achieved in the Instron capillary rheometer with the extrusion procedure devised originally by Southern and Porter.[5,6] Indeed, the high-density polyethylene filaments prepared by their technique surpass all conventionally processed polyethylenes in crystalline orientation,[12] chain extension,[13–15] tensile modulus,[16,17] and tensile strength.[17] The results of the Southern and Porter

Journal of Applied Polymer Science, Vol. 22, 163–185 (1978)

0021–8995/78/0022–0163$01.00

experiment with polyethylene have prompted many questions, among them: How will a different polymer with higher melting point and lower degree of crystallizability respond to high-pressure extrusion in a capillary die? Moreover, can the ordering potential of converging melt flows be harnessed for a polymer of well-established value as a fiber former?

In the present work, the generality of the rheometer extrusion procedure for the production of unique fibrous morphologies has been tested with poly(ethylene terephthalate) (PET). The procedure of Southern and Porter was used to extrude PET under high pressure over a wide range of temperatures and times. A significant outcome of the work was the production of highly oriented, translucent segments directly from polymer melt. Then, the structural properties of the extruded segments were examined by wide-angle and small-angle x-ray scattering, density determinations, differential scanning calorimetry, hot-stage optical microscopy, and shrinkage measurements. Particular attention was directed toward an understanding of the effect of temperature and time on the properties of the translucent segments.

MATERIALS AND METHODS

Extrusion Procedure

An Instron capillary rheometer was used to perform the high-pressure extrusion experiments. A tungsten–carbide capillary die, 2.55 cm long with a diameter of 0.127 cm and a 90° entrance angle, was used in all experiments.

A melt-polymerized PET, Goodyear VFR 2585A, was used exclusively in the extrusion experiments. The as-received polymer chips have a nominal intrinsic viscosity of 0.95 dl/g ($M_n = 3.7 \times 10^4$).

To minimize hydrolytic degradation of the PET sample on melting, we dried the chips under vacuum (0.1 mm Hg) at 142°C for 18–24 hr. Dow–Corning 550 silicone oil was used as an extrusion lubricant. A thin film of silicone oil was applied to the walls of a rheometer barrel before the polymer chips were loaded. The chips were melted in the rheometer reservoir at 285°C for 5 min. Then, the temperature was lowered to the desired value. In the present work, extrusion experiments were conducted at temperatures from 245° to 265°C. Once the desired extrusion temperature was attained, the plunger speed was increased in fixed increments with the use of the push-button speed selector. At each successive plunger speed, sufficient time was allowed for pressure equilibrium to be achieved.

Ultimately, however, a "critical" plunger speed was attained at which the extrusion pressure did not level off. Instead, once the "critical" plunger speed was initiated, one of two possible types of pressure phenomena would occur. The pressure could rise rapidly to about 1400 atm and begin to fluctuate irregularly. The nature of the pressure oscillation phenomenon along with the properties of the toroidal crystalline aggregate which forms during pressure oscillation are the topics of a separate paper.[18] In the alternative pressure phenomenon, the pressure would rise rapidly without oscillation to the instrumental limit of the rheometer. The present work is concerned solely with extrusion experiments which were preceded by the nonoscillatory type of pressure behavior.

The pressure trace shown in Figure 1 illustrates the procedure used to extrude

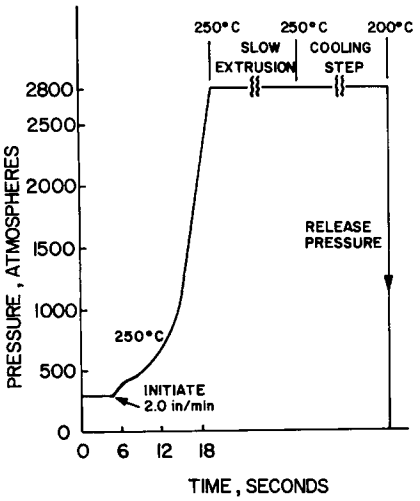

Fig. 1. Instron pressure trace illustrating the procedure used to prepare PET segments by high-pressure extrusion.

PET under high pressure. The extrusion procedure is basically similar to the procedure used by Southern and Porter[6] to prepare ultraoriented segments of high-density polyethylene. During the pressurization step, the pressure rose rapidly to the rheometer limit and the extrusion rate dropped drastically. Southern and Porter concluded that the nonequilibrium pressure trace resulted primarily from the massive crystallization of polyethylene melt in the rheometer reservoir. In the present experiments with PET, however, massive crystallization did not appear to play a dominant role in the pressurization step. The high rates at which the pressure rose to the instrumental limit were inconsistent with a crystallization mechanism, because PET melts crystallize slowly at temperatures approaching the melting point.[19,20] Rather, the rapid ascent of the extrusion pressure probably resulted from the elastic compression of melt in the rheometer reservoir under the high-impact loads which were applied.[21,22] After the pressurization step, the load-cycling capability of the rheometer was used (at a low plunger speed) to maintain the pressure between 2700 and 2900 atm. During the load-cycling step, the melt in the rheometer reservoir was cyclically compressed and decompressed and thereby maintained in a state of nonequilibrium. Load cycling was essential for pressure maintenance during the initial stages of extrusion. While the pressure was isothermally maintained about the 2800-atm mean, a cylindrical segment was slowly extruded into the capillary. After the desired extrusion time, the rheometer was cooled to 200°C at about 2°C/min. Then the pressure was released, and the solid capillary strand (0.125 cm diameter) with attached reservoir-plug (0.95 cm diameter) was removed as a unit from the rheometer.

The extent of polymer degradation in the rheometer reservoir was frequently checked through the determination of the intrinsic viscosity $[\eta]$ of extrudate and reservoir-plug samples gathered at different times in the extrusion procedure. Intrinsic viscosities were determined at 30.0°C in a 60–40 (wt-%) mixture of phenol and tetrachloroethane. Figure 2 shows the variation of $[\eta]$ with residence time for several experiments in which the final extrusion temperature was 260°C.

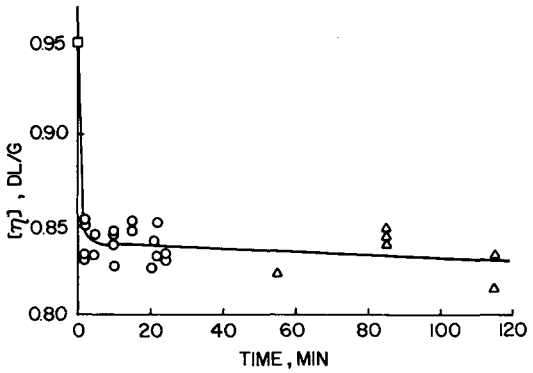

Fig. 2. Effect of residence time in high-pressure extrusion experiment on intrinsic viscosity of PET samples. The completion of the chip-loading step at 285°C was arbitrarily taken as zero time, and the final extrusion temperature was 260°C: (□) chip (as received); (○) extrudate; (△) reservoir plug.

After the polymer chips were melted (first 5 min) and the melt was cooled to 260°C (next 15–20 min), the melt was pressurized and extruded under high pressure. From degradation studies of polyester melts, Marshall and Todd[23] and Wampler and Gregory[24] concluded that complete and virtually instantaneous hydrolysis occurs before the onset of thermal degradation. Therefore, in the present experiments, the initial, precipitous drop of $[\eta]$ from 0.95 dl/g to an average value of 0.84 dl/g ($\overline{M}_n = 3.1 \times 10^4$) probably resulted from rapid hydrolytic degradation of the PET melt. Furthermore, the slow, linear decline of the molecular weight after the initial hydrolysis step was probably caused by the slow process of thermal degradation. We conclude that the PET segments prepared in the present study were materials of high molecular weight.

X-Ray Scattering Experiments

Ni-filtered CuK_α radiation from a Rigaku–Denki rotating anode generator was used in all x-ray experiments. Wide-angle x-ray scattering (WAXS) photographs were taken on a flat-plate camera with a sample-to-film distance of 5 cm. The diameter of the impinging beam was about 0.55 mm. In all experiments the x-ray beam was directed normal to the segment axis. The WAXS photographs were scanned azimuthally around the (100) and (010) equatorial reflections with a Joyce–Loebl microdensitometer equipped with a polar table. The background for each reflection was established from two azimuthal scans made at positions differing by about 1.0° from the Bragg angle for the reflection peak.

Small-angle x-ray scattering (SAXS) photographs were taken on a Rigaku-Denki small-angle camera with a sample-to-film distance of 300 mm. The x-ray beam was sequentially collimated by two pinholes 0.5 mm and 0.3 mm in diameter. Long periods were calculated with Bragg's equation after correction of the meridional microdensitometer scans for background scattering.

Density Determinations

The densities of the extruded segments were determined at 23.0° ± 0.2°C in a density gradient column containing a calcium nitrate–water solution. Crys-

tallinity values were calculated from the density data through the relation

$$X = \rho - \rho_a/\rho_c - \rho_a$$

where X is the volume crystalline fraction, ρ is the sample density, ρ_a is the amorphous density (1.335 g/cm^3), and ρ_c is the crystalline density (1.455 g/cm^3). The computed crystallinities were used only to determine relative changes in crystallinity and should not be regarded as absolute values.

Differential Scanning Calorimetry

The melting behavior of the extruded segments was investigated with a Perkin–Elmer differential scanning calorimeter (DSC) Model 1B. The DSC was calibrated at 232°C with a tin standard. A heating rate of 20°C/min and a sample mass between 3 and 4 mg were used in all tests. The samples were disks about 0.5 mm thick, which had been sliced from cylindrical segments with a miniature lathe. Use of the disk geometry ensured good thermal contact between the sample and sample pan and thereby minimized instrumental heat lags.

Hot-Stage Optical Microscopy

A Unitron polarizing microscope equipped with a Kofler micro hot stage was used for the melting studies. The hot stage was calibrated at 244.0° and 336.0°C with calibration crystals included with the apparatus. Longitudinal thin sections from the oriented segments were observed at a heating rate of about 2°C/min. An unoriented PET extrudate was oven annealed at 200°C for 30 min and was included in the study as a spherulitic control sample. Immersion liquids were not used in the hot-stage experiments.

Shrinkage Measurements

Segments from 1 to 4 mm in length were immersed in a silicone oil bath for 1 hr at temperatures up to 270°C. The temperature of the oil bath was controlled to ±0.5°C. The segments were annealed in individual Teflon pouches which minimized the frictional resistance to shrinkage. After immersion in the oil bath, we quenched the annealed segments in carbon tetrachloride to remove the oil. A miniature lathe equipped with a precision razor-blade tool was used to cut flat-end segments from the capillary strands. The initial and final lengths, l_0 and l, of the segments were measured with a micrometer. The shrinkage S was expressed as $(l_0 - l)/l_0$.

RESULTS AND DISCUSSION

Segment Appearance and Growth

All short-growth segments prepared by high-pressure extrusion at temperatures from 245° to 265°C were translucent to visible light. Figure 3 shows the typical appearance of the capillary strand with attached entrance-cone plug after removal from the rheometer and capillary die. The entrance cone is at the extreme right of the photograph and is opaque. However, a translucent segment,

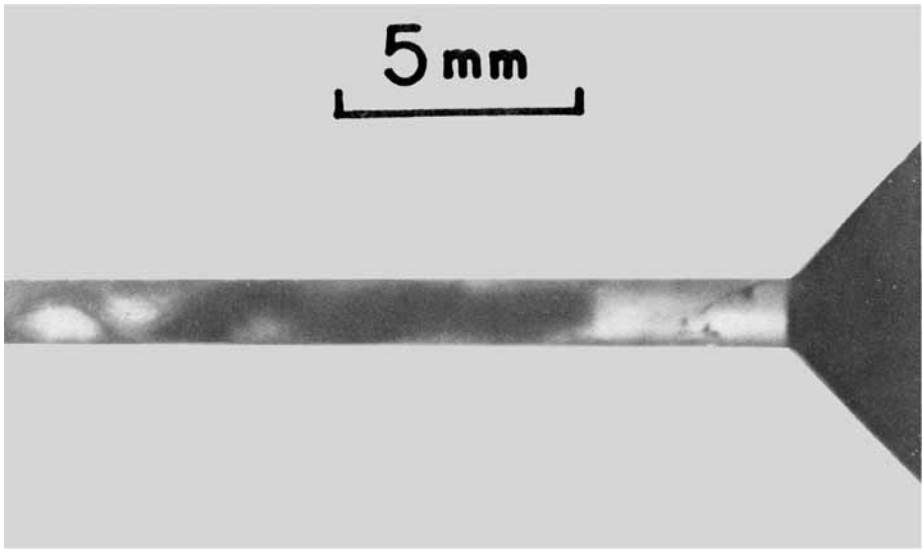

Fig. 3. Transmission optical micrograph of PET capillary-strand (1.25 mm diameter) recovered from the rheometer after high-pressure extrusion for 30 min at 260°C.

about 4 mm long, is located immediately adjacent to the opaque entrance cone. This 4-mm segment formed during the maintenance of 2800 atm at 260°C for 30 min. The translucency of the short-growth segments increased noticeably as the extrusion temperature was raised. Segments prepared at 265°C were exceptionally translucent.

Although the properties of translucent segments located adjacent to the capillary entrance are the main topic of the present study, Figure 3 shows another interesting region of the capillary strand which deserves mention. Located to the left of the 4-mm translucent segment is a 10-mm segment which consists of an opaque, undulating streak embedded in a matrix of translucent polymer. In three dimensions, the undulating streak is a continuous, large-pitched helix which becomes progressively more diffuse in appearance at positions closer to the entrance end of the capillary strand. WAXS photographs of this unusual segment showed that the c-axis of the crystals was tilted at about 15° to the strand axis. The helical crystallization pattern probably resulted from crystallization during the spiralling flow[25] of highly viscoelastic PET melt into the capillary. The polymer melt must have swirled into the capillary during the pressurization step in the extrusion procedure. The diminution of helix clarity reflects the flow rate decrease which occurred as the pressure rose to 2800 atm.

The highly directional nature of the translucent segment morphology became readily apparent when the segments were crushed or split. When struck perpendicular to the longitudinal axis, the segments would splay into axially oriented fibrous bundles. The segments could be easily peeled parallel to the longitudinal axis by the method of Scott.[26] The scanning electron micrograph in Figure 4 shows a chord peel which reveals the fibrillar morphology of the translucent segment.

The length of a translucent segment which formed in a given time was strongly influenced by extrusion temperature, as Figure 5 shows. The translucent segment length which formed in 30 min increases from only ¼ mm at 245°C to a

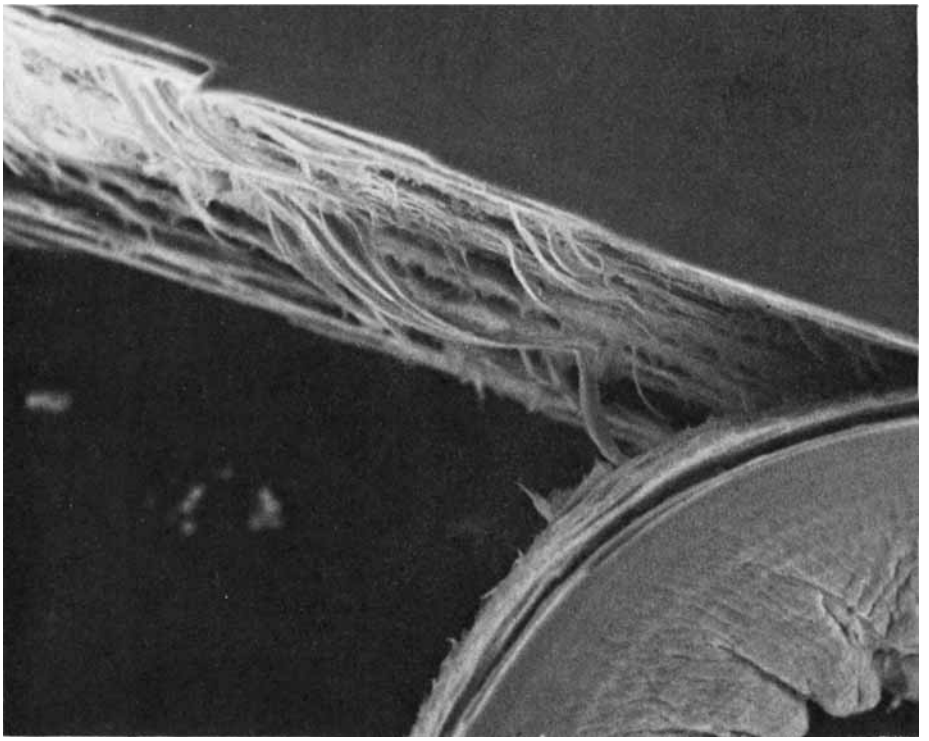

Fig. 4. Scanning electron micrograph of a longitudinally peeled segment of translucent PET prepared at 262°C by high-pressure extrusion. Magnification 100 times.

maximum of almost 4 mm at 260°C. However, at temperatures above 260°C, the translucent segment length decreases sharply. In contrast, Figure 6 shows that the mass of extrudate which is displaced from the capillary exit in 30 min increases sharply as the extrusion temperature is raised above 260°C. This comparison readily points out a major limitation of the present extrusion technique with the capillary die: the translucent segments melted partially in the capillary at the higher extrusion temperatures.

The extent of segment melting at 262° and 265°C was estimated from the data of Figures 5 and 6. We converted the values of extrudate mass from Figure 6 into equivalent segment lengths, after assuming a segment density of 1.40 g/cm^3.

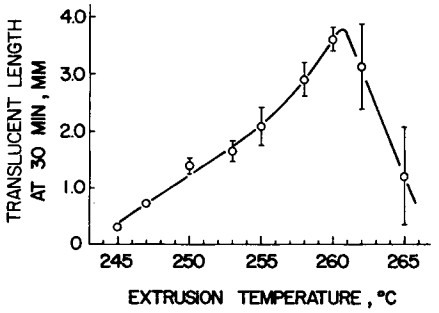

Fig. 5. Effect of extrusion temperature on translucent segment length formed during high-pressure extrusion of PET for 30 min. Bars denote 0.90 confidence intervals for the means.

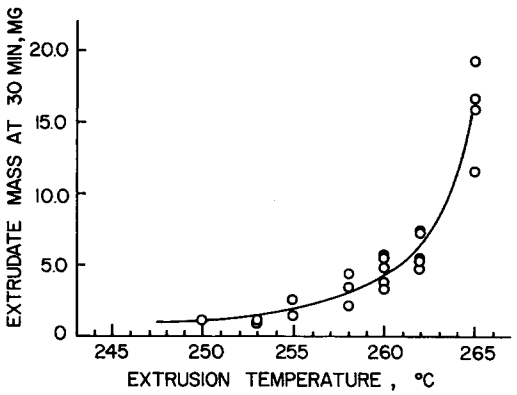

Fig. 6. Effect of extrusion temperature on extrudate mass displaced from the capillary during high-pressure extrusion of PET for 30 min.

At 265°C, the computed segment length was about 10 mm, but Figure 5 shows that the average actual length of the translucent segments was only about 1 mm. Thus, the length reduction due to melting at 265°C was about 90%. At 262°C, the length reduction was about 25%. Therefore, while the stretching field in the conical entrance served to form the translucent morphology, the capillary served merely as a pressure quencher whose effectiveness for preserving the translucent morphology diminished as the extrusion temperature was raised above 260°C.

The nature of the growth of the translucent segments with time provided preliminary information which suggested that the high-pressure extrusion of PET by the standard procedure of Southern and Porter was controlled by the time-dependent crystallization of melt in the rheometer reservoir. Figure 7 shows that the segment growth curves at 250°, 255°, and 260°C display the same basic features. During the initial stages of segment growth under 2800 atm, the extrusion rate, which may be evaluated from the slope of the growth curves, decreases slowly with time. However, the extrusion rate eventually attains a highly temperature-dependent value that remains constant with time. The obvious conclusion is that the time-dependent variation of the extrusion rate is associated with a gradual change of state of the polymer in the rheometer reservoir.

The segment growth curves in Figure 7 imply the existence of two growth mechanisms: (a) flow-induced crystallization during the early stages of extrusion, followed by (b) solid-state extrusion. The linear increase of segment length with time displayed in each growth curve is a characteristic feature of the solid-state extrusion of polymers under constant pressure.[27] The extrusion rate in the steady-state portion of the experiment showed a strong dependence on temperature: the extrusion rates were 0.037, 0.006, and 0.002 mm/min at 260°, 255°, and 250°C, respectively. The steady-state rate of extrusion was also affected by friction at the polymer–metal interface in the rheometer reservoir, an observation which is again consistent with a deformation mechanism via solid-state extrusion. Extrusion experiments were performed at 255°C with and without the use of a silicone oil lubricant on the walls of the rheometer reservoir, and the growth results were compared. Figure 8 shows that the extrusion rate during the first 5 min of the experiment was virtually unaffected by the absence

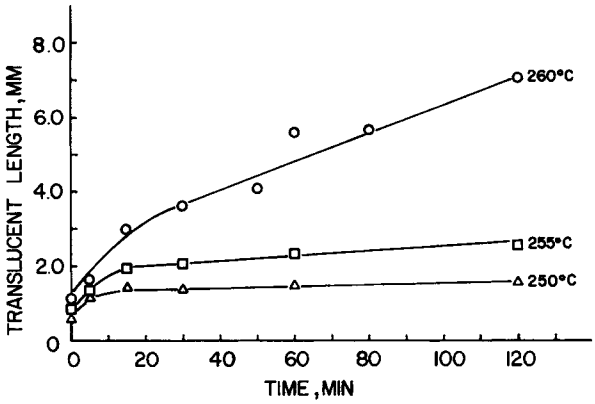

Fig. 7. Translucent segment length as a function of time during high-pressure extrusion of PET at 250°, 255°, and 260°C.

of lubrication, apparently because segment formation occurred by the crystallization of oriented melt. Yet without the benefit of reservoir lubrication, segment formation stopped entirely after the initial period of rapid growth.

The dual mechanism hypothesis of PET segment formation is further supported when the growth curves in Figures 7 and 8 are compared with the growth behavior reported by Southern and Porter for transparent polyethylene segments at constant temperature and pressure. An initial stage of decreasing extrusion rate was not observed by Southern and Porter for extrusion of polyethylene under 1900 atm at 136°C. The segment length was shown to be a linear function of time throughout the extrusion experiment. The difference between the segment growth curves of these two polymers is probably related in large measure to a difference in their rates of crystallization at comparable degrees of supercooling. Southern et al.[28] concluded that the polyethylene sample crystallized massively in the rheometer reservoir during the pressurization step at pressures exceeding about 600 atm. Therefore, the extrusion of ultraoriented polyethylene is a solid-state deformation even during the initial stages of the experiment.[14] With PET, however, the complete transformation of supercooled melt into solid must necessarily be delayed because of the low crystallization rate of this polymer.

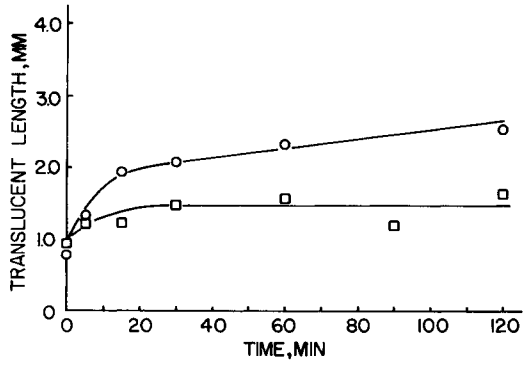

Fig. 8. Effect of silicone-oil lubrication on translucent segment growth during high-pressure extrusion of PET at 255°C: (○) with lubrication; (□) without lubrication.

Effect of Time on Segment Properties

The observed dependence of extrusion rate on time implied that the properties of the PET segments should change with time. The effect of time on segment properties was investigated through a positional examination of long segments prepared in prolonged extrusion experiments at 260°C. The lengths of the segments after extrusion times of 180, 300, and 480 min were 9.8, 11.7, and 22.0 mm, respectively. In all measurements, the capillary entrance was designated as the zero position.

It soon became apparent that the translucence of each long-growth segment changed with axial position and, therefore, with time. To determine the variation of light transmittance with axial position, we scanned along the length of each 24-mm capillary strand using a Joyce–Loebl microdensitometer equipped with translation table. The resultant microdensitometer scans provided an expeditious means of visualizing the course of the extrusion experiment. Figure 9 shows that three regions may be delineated in the capillary strands on the basis of light transmission. Region 1 is composed predominately of opaque material which occupied the capillary before the start of extrusion at 2800 atm. The material in region 1 was forced from the capillary as extrusion progressed. Regions 2 and 3 were formed during high-pressure extrusion at 2800 atm for the indicated time. Region 2 is a 7-mm segment of variable translucence which formed first in the extrusion experiment. As the axial distance decreases in each scan of region 2 (i.e., as time increases), the optical density decreases to a minimum value and then increases gradually. Region 3 is composed of virtually opaque material which forms during the remainder of the extrusion experiment.

In summary, we see from the microdensitometer scans that the formation of the translucent morphology stopped after a certain time. Subsequently, the

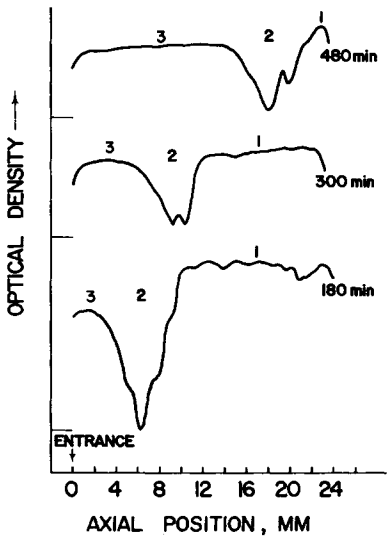

Fig. 9. Axial microdensitometer scans of capillary strands formed during high-pressure extrusion of PET at 260°C for 180, 300, and 480 min.

7-mm translucent segment was forced as a solid plug toward the capillary exit by the formation of a segment of uniform opacity.

The crystalline orientation of the long-growth segments was also examined as a function of axial position. WAXS photographs were taken with the x-ray beam targeted at accurately measured distances from the capillary entrance. Of the three prominent equatorial reflections in the WAXS patterns, the (100) reflection displayed the most sensitivity to changes in axial position. Thus, for the purpose of comparison, the width at half-maximum intensity of the (100) reflection, $\phi(100)$, was used as an empirical index of the degree of c-axis orientation.

The crystalline orientation as indicated by $\phi(100)$ proved to be a sensitive and reliable fingerprint of the structure that had formed originally at the capillary entrance during the extrusion experiment, because the orientation was essentially unaffected by the annealing treatment in the capillary. The curves showing the systematic change of $\phi(100)$ with axial position are given in Figure 10. The orientation curves provide startlingly good confirmation of the time dependence of the extrusion process with PET. Over a 3- to 4-mm region at the exit end of each segment, the orientation is high and goes through a slight maximum. The position of the orientation maximum in each curve of Figure 10 roughly corresponds to the position of the optical density minimum in each region-2 scan of Figure 9. After the region of high orientation in Figure 10, the orientation decreases over a length of about 4 mm as the axial distance decreases. The gradual decline of orientation in each curve corresponds to the gradual rise of optical density in each microdensitometer scan of region 2. Finally, the orientation reaches a low value which remains constant with position (and time); this low-orientation material is the region-3 material of Figure 9.

Figure 11 shows the typical progression of the (100) azimuthal intensity profile as a function of position along the long-growth segments. In the translucent portion of the segment formed at 300 min, the intensity profile broadens gradually about the equator as the axial distance decreases. Finally, at the 5.0-mm position and at all positions in the opaque portion of the segment, the (100) reflection splits, with peak maxima separated from the equator by about 10°. Of

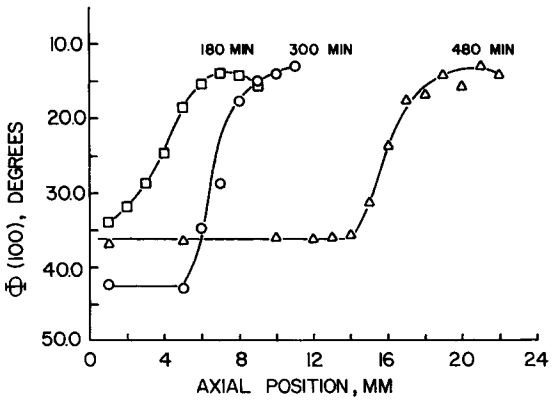

Fig. 10. Width of half-maximum intensity of the (100) reflection as a function of axial position for PET segments formed during high-pressure extrusion at 260°C for 180, 300, and 480 min. The capillary entrance is the zero position.

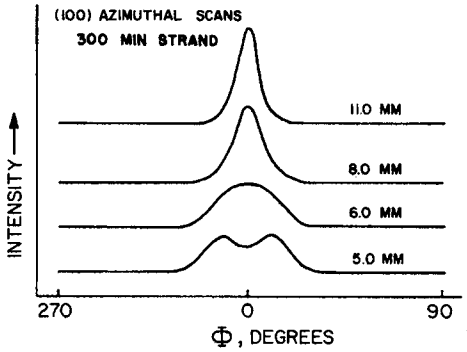

Fig. 11. Azimuthal intensity profiles of the (100) reflection as a function of axial position for a PET segment formed during high-pressure extrusion at 260°C for 300 min.

the other equatorial reflections in the WAXS pattern of the opaque material, the $(1\bar{1}0)$ reflection also split at about 10°, while the (010) intensity peak remained on the equator. Thus, the (100) split signifies that the c-axis of the crystals in the opaque material was preferentially tilted with respect to the extrusion direction. Crystal tilt is common in PET films and fibers which have been plastically deformed to low elongations and annealed subsequently under restraint.[29–31]

The effect of time of the isothermal extrusion of PET under high pressure is best portrayed in Figure 12, where the orientation curves of Figure 10 have been placed on a logarithmic time scale. The length–time curve for extrusion at 260°C (Fig. 7) was used to convert the axial position values in Figure 10 into corresponding values of time. The orientation–time curves for the 180-min and 480-min strands superimpose completely, but the curve for the 300-min strand superimposes only over the initial 20 min of extrusion. Excessive friction at the walls of the rheometer reservoir, due to the presence of residue or improper lubrication, was undoubtedly responsible for the reduced growth of the 300-min strand in the latter stages of extrusion. Nevertheless, the basic shape of the curves in Figure 12 is the same. Their sigmoidal shape bears more than a superficial resemblance to the crystallization isotherms which are so characteristic

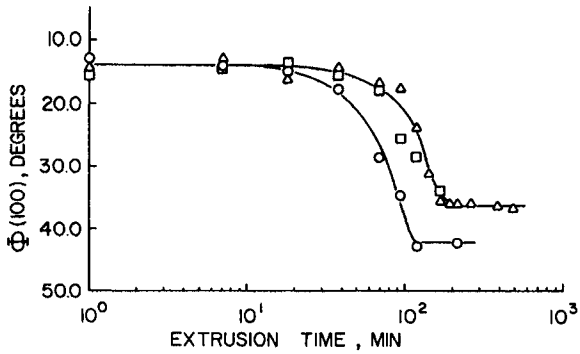

Fig. 12. Width at half-maximum intensity of the (100) reflection as a function of time for PET segments formed during high-pressure extrusion at 260°C for (□) 180, (○) 300, and (△) 480 min. Demonstration of the superposability of the curves in Fig. 10.

of the quiescent crystallization of polymers.[20,32] Indeed, the orientation–time curves appear to be unique crystallization isotherms in which the crystal orientation is used as a sensitive detector of the liquid-to-solid transformation in the rheometer reservoir under high pressure because the orientation which was imparted under constant pressure in the conical entrance of the capillary die was dependent upon the ductility or compliance of the flowing polymer. The ductility was, in turn, dependent upon the extent of the phase transformation in the rheometer reservoir.

When viewed as crystallization isotherms, the orientation–time curves in Figure 12 may be used to more precisely analyze the extrusion process in terms of possible mechanisms and microstructure. The initial portion of the curves, in which the orientation is high and unchanging, represents a period of induction. Accordingly, the quiescent melt in the rheometer reservoir must have failed to crystallize to a detectable extent during the first 20–30 min of the experiment. The crystallization process was probably retarded by the high rates of compression which were imposed during pressurization and load cycling.[33] Presumably, the sudden compressions greatly impeded the diffusion of chain segments in the quiescent melt and thereby increased the time required for crystalline embryos to reach critical size. Therefore, during the induction period, the polymer chains in the highly compliant melt were aligned by the extensional and shear flow fields in the conical entrance region. We propose that the prealigned chains then crystallized in the vicinity of the capillary entrance and served as nuclei for lamellar growth perpendicular to the segment axis. Because of the high extrusion temperatures, the lamellar growth should have been rapid once the fibrous nuclei were provided by the flow at the capillary entrance.

The obvious model for the microstructure of the translucent material which formed during the induction period is the row structure proposed by Keller and Machin.[34] Conventional preparation procedures such as fiber spinning appear to be ineffective for the production of row-nucleated structures from PET melts, as Spruiell et al.[35] have pointed out. Yet in the present extrusion method, the flow rate and the crystallization rate were more closely matched so that crystallization could accompany orientation. After the induction period, the orientation decreases at an accelerating rate. The rapid decrease in orientation probably reflects the rapid decrease in the compliance of the reservoir material as crystallization progressed autocatalytically. The dominant microstructure of the extruded segment would again be the row structure because flow-induced crystallization would still be the dominant mechanism. However, as the solidification process neared completion, the flow-induced crystallization mechanism must have gradually given way to the plastic deformation of pressure-induced spherulitic structure in the rheometer reservoir. Figure 12 shows that the orientation finally leveled off once the solidification process was completed. Segment growth then proceeded exclusively by the solid-state extrusion of reservoir material whose ductility remained low and constant with time.

We conclude from Figures 9 to 12 that a spectrum of oriented microstructures was present along the length of the PET segments prepared by high-pressure extrusion. This conclusion is in sharp contrast to the results obtained in the original extrusion experiments with polyethylene. Southern and Porter reported that the clarity and crystalline orientation of their transparent segments were time insensitive.

Effect of Temperature on Segment Properties

Because of the marked dependence of segment orientation on axial position, the study of the temperature dependence of certain properties was confined to translucent segments which formed within the first 30 min of the extrusion experiment. Figure 12 shows that segments which formed during the initial stages of extrusion should be the most structurally homogeneous. Several properties of segments prepared at different temperatures in the 250–265°C range were investigated: (a) crystalline orientation, (b) lamellar orientation and magnitude of long periods, (c) degree of crystallinity, and (d) melting behavior.

The effect of extrusion temperature on crystalline orientation was determined for translucent segments which had formed during an extrusion time of 30 min. We also checked the orientation homogeneity within each segment by taking WAXS photographs with the x-ray beam targeted at different axial positions. The widths of the (100) and (010) azimuthal intensity profiles at half-maximum intensity were averaged, and the resultant value, $\phi(^{100}_{010})$, was used as an empirical index of the degree of alignment. Table I summarizes the results of the orientation analysis. As expected, the orientation of translucent segments prepared at each temperature was position dependent. However, the range of the orientation variability within each segment was not large. Table I also shows that the most highly oriented material was prepared at 265°C, despite the severe effect of postextrusion melting at this temperature.

The WAXS pattern of the segment prepared at 265°C is shown in Figure 13a. This fully developed fiber pattern documents the high orientation which is achievable in controlled converging flows. Segments extruded at temperatures below 265°C were also highly oriented and had roughly equivalent orientation values, as Table I shows. The sharp increase of crystalline orientation at temperatures above about 262°C is understandable in light of a similar trend exhibited by the mass flow rate results shown in Figure 6. The apparent correlation between crystalline orientation and flow rate points again to a hydrodynamic mechanism of segment formation during the initial stages of the extrusion experiment. Apparently, the highest degree of chain alignment was achieved at 265°C because the highest longitudinal velocity gradient was generated in the conical entrance region at this temperature. Unfortunately, the limitations of

TABLE I
Axial Variability of Crystalline Orientation Determined by Wide-Angle X-Ray Scattering for Translucent PET Segments Prepared at Different Extrusion Temperatures

Extrusion temp., °C	Segment length,[a] mm	$\phi(^{100}_{010})$,[b] degrees		
		Minimum	Mean	Maximum
253	1.5	13.8	14.5	15.2
255	2.2	12.1	12.6	13.2
258	3.0	13.0	13.5	14.4
260	3.6	12.6	14.1	16.0
262	3.0	13.8	15.1	16.7
265	1.6	11.0	11.2	11.5

[a] Extrusion time, 30 min.

[b] $\phi(^{100}_{010})$ is the average of the widths of the (100) and (010) azimuthal profiles at half-maximum intensity.

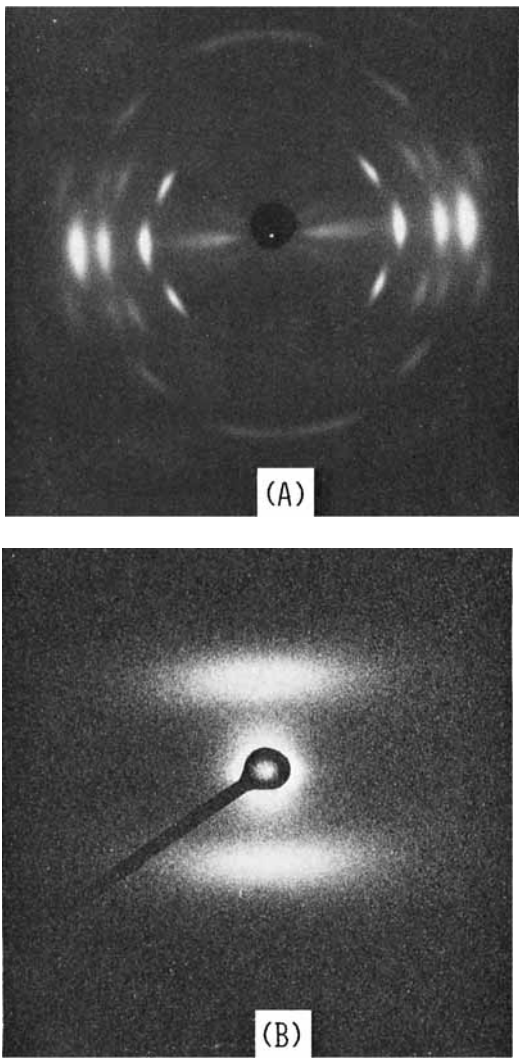

Fig. 13. (a) Wide-angle and (b) small-angle x-ray scattering patterns of a translucent PET segment prepared by high-pressure extrusion at 265°C. Extrusion direction is vertical.

quenching with high pressure prevented complete exploitation of the high chain alignment achieved at 265°C.

The SAXS patterns from translucent segments were also examined as a function of extrusion temperature. Short-growth (30 min) segments prepared at temperatures from 250° to 265°C gave scattering patterns similar to the one shown in Figure 13b. The strong meridional maxima show that the fundamental scattering units of the translucent segments are parallel microfibrils, presumably row-nucleated cylindrites, composed of alternating regions of crystalline and amorphous material.[36] The line-type shape of the discrete maxima suggests that the basal planes of the stacked lamellae possess some waviness.[37] Yet, on the average, the basal planes of the lamellae should be oriented perpendicular to the segment axis—a conclusion consistent with the row model proposed previously for the segment microstructure. The lamellae are arranged differently

TABLE II
Long Periods of Translucent PET Segments[a] as a Function of Extrusion Temperature

Extrusion temp., °C	Long period, Å
250	130
253	132
255	138
258	135
260	133
262	141
265	140

[a] Extrusion time, 30 min.

within conventionally processed PET yarn, since drawn yarns usually show a four-point SAXS pattern.[38,39] The four-point pattern implies that the lamellar basal planes are oriented at an oblique angle to the fiber axis.[37] As in other plastically deformed polymers,[40] the lamellar tilt in PET yarn may be related to the flow pattern in the neck during deformation. A four-point pattern was never recorded in the scattering experiments with the translucent segments.

The magnitudes of the long periods of the translucent segments were within the characteristic range for drawn PET fibers[41] and showed only a slight dependence on extrusion temperature. Table II shows that the long period increased only 10 Å for a 15°C increase in extrusion temperature. The slight increase in long period was probably associated with the annealing process in the capillary after row-nucleated growth. The relative insensitivity of the long period of the PET segments to extrusion temperature contrasts sharply with the SAXS results of Weeks et al.[14] for ultraoriented polyethylene. Their findings were consistent with a formation mechanism involving plastic deformation because the long period of the ultraoriented strands increased 65 Å for only a 4°C increase in extrusion temperature.

The effect of extrusion temperature on segment crystallinity was determined for (a) samples which formed when the cooling step was initiated immediately after the pressure rose to 2800 atm, and (b) samples which formed during an extrusion time of 30 min. The density crystallinities of the translucent segments are plotted against extrusion temperature in Figure 14. For both sets of test samples, the plots are identical in shape, but are displaced from one another along the crystallinity axis. Crystallinity increases linearly with extrusion temperature over the 250–260°C range. However, at temperatures above 260°C, the crystallinity values reach a saturation level, presumably because of a partial melting phenomenon in the capillary.

Figure 14 clearly shows that the translucent segments were extensively annealed during growth down the capillary. During segment growth at all temperatures, the crystallinity of the initial segment increases by about 7% after 30 min. Figure 14 also shows that the high-pressure annealing treatment yielded a highly crystalline product. Segments prepared at temperatures of 260° to 265°C with an extrusion time of 30 min had a density of 1.410 g/cm^3, which corresponds to a crystallinity of about 62%. To obtain a comparable density value, Holdsworth and Turner-Jones[42] annealed their bulk PET samples at 240°C for 960 min.

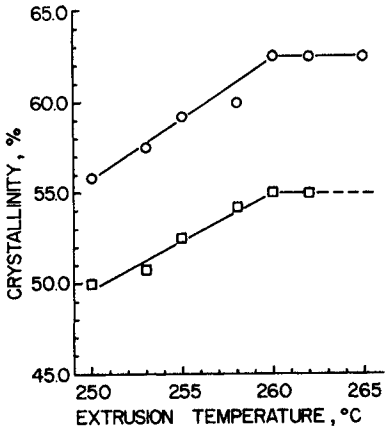

Fig. 14. Effect of extrusion temperature on the crystallinity of translucent PET segments formed during high-pressure extrusion for zero min (immediately cooled) (□) and 30 min (○).

Finally, we examined the melting behavior of translucent segments prepared at different extrusion temperatures. The typical shapes of the melting endotherms of the short-growth (30 min) segments are shown in Figure 15. Some justification should first be given for the belief that these single-peak endotherms are directly related to the state of the translucent segment before the melting experiment. The work of several investigators[42–46] has generally clarified the mechanisms which are involved in the structural reorganization of PET samples during calorimetric measurements. It is clear that PET samples must be annealed at high temperatures for sufficient times before the double endotherms indicative of recrystallization phenomena give way to a single endotherm which is characteristic of the original crystallization conditions. The single endotherm, which is commonly referred to as a form-II peak, apparently arises because the annealed sample solely contains larger and more perfect crystals which are unable to recrystallize after they melt during the heating scan.[45] Similarly, we believe that the DSC curves in Figure 15 are form-II endotherms, because the time, temperature, and pressure conditions of the extrusion experiment should have been more than sufficient to produce nonrecrystallizable material. The high

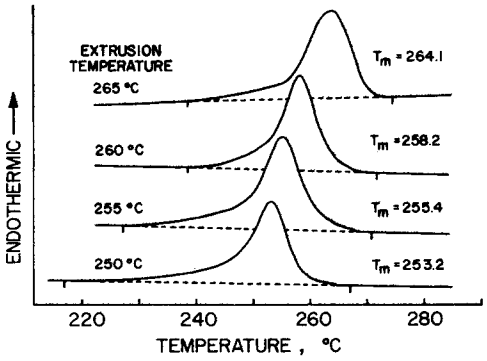

Fig. 15. DSC melting endotherms of translucent PET segments formed during high-pressure extrusion at 250°, 255°, 260°, and 265°C for 30 min. DSC heating rate was 20°C/min.

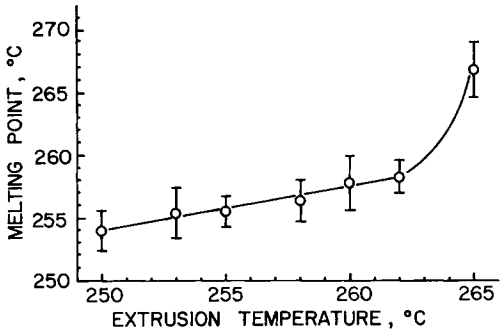

Fig. 16. DSC peak melting point as a function of extrusion temperature for translucent PET segments formed during high-pressure extrusion for 30 min. DSC heating rate was 20°C/min. Bars denote 0.95 confidence intervals for the means.

densities of the translucent segments certainly attest to the relative perfection of their crystalline components. Furthermore, the high scan rate (20°C/min) should have suppressed the recrystallization phenomenon.[45]

Figure 15 shows that melting range decreases, and the peaks of the endotherms shift progressively to higher temperatures as the extrusion temperature increases. A large shift in the melting peaks occurs as the extrusion temperature increases from 260°C to 265°C. The distinctive, high-melting character of the segments prepared at 265°C is readily apparent in Figure 16, where the melting peak temperatures are plotted as a function of extrusion temperature. Each datum point is the average of at least four tests. As the extrusion temperature increases from 250° to 262°C, the average melting point increases only about 4°C. However, from 262° to 265°C, the melting point increase is almost 9°C.

For translucent segments prepared at temperatures below 262°C, the dominant factors controlling thermal properties may be crystal size and perfection. But the small increases in long period (Table II) and density (Fig. 14) with extrusion temperature are not sufficient to account for the large change in melting behavior above 262°C. Yet the melting point results in Figure 16 do correlate with the flow rate (Fig. 6) and crystalline orientation (Table I) measurements, since the latter variables also increase sharply as the extrusion temperature is raised above 262°C. Perhaps the higher longitudinal velocity gradient in the conical entrance region at 265°C generated a high degree of chain continuity which resulted in a highly constrained chain network in the extruded segments. During the melting experiment, the stable tie points of the strained network would have hindered the randomization of molten polymer. Hence, at a given heating rate, the melting point would have been raised because the entropy gain on melting would have been temporarily restricted. The phenomenon of temporary entropy restriction has been demonstrated experimentally by Miyagi and Wunderlich[47,48] for bulk PET samples and PET filaments.

Hot-Stage Optical Microscopy

Grubb et al.[49] have recently demonstrated the utility of the polarizing microscope equipped with a hot stage for the detection of fibrous crystals in bulk polymer samples prepared by different methods of orientation crystallization.

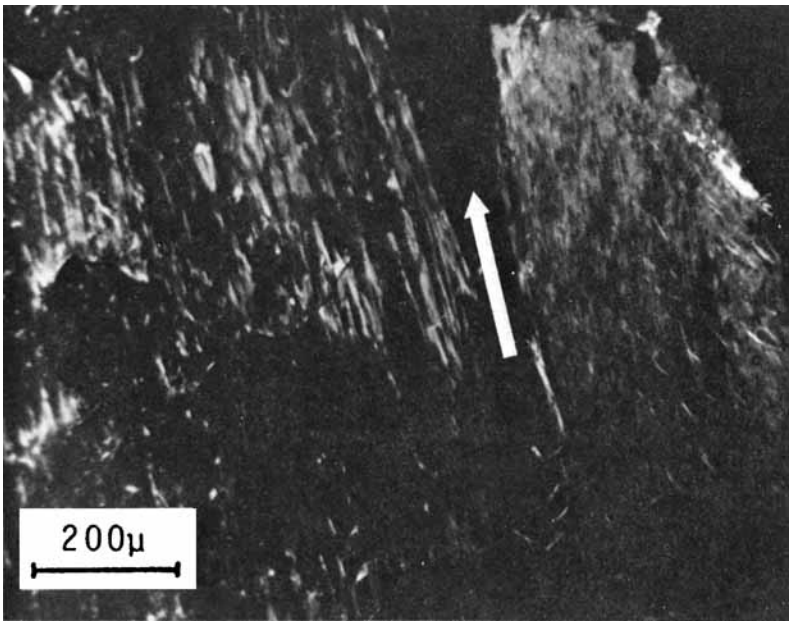

Fig. 17. Optical micrograph (crossed polars) of PET fibrous crystals from a longitudinal thin section of a translucent segment formed during high-pressure extrusion at 260°C for 30 min. Hot-stage temperature is 267°C. Arrow denotes the extrusion direction.

Visual examination of the melting behavior of the translucent PET segments was also useful in the present work. Translucent segments prepared at 260°C with an extrusion time of 30 min were examined.

The main events in the melting process of the translucent segments were highly reproducible. The appearance and shape of the thin section remained unchanged at temperatures up to about 260°C. However, at about 264°C, small droplets of melt began to form as the sample softened. At about 266°C, the thin section collapsed under the weight of the coverglass, and a profusion of strongly birefringent, fibrous crystals suddenly appeared which were oriented parallel to the extrusion direction. Only 1°–2°C higher, at about 267°C, the sample appearance again changed drastically. The brilliant polarization colors departed, and, as Figure 17 shows, distinct bundles of long fibrils appeared. Most of the fibrils possessed first-order white birefringence and were embedded in a matrix of isotropic melt. Upon continued heating, the fibrils slowly disappeared. The birefringence of fibrils from the translucent segments persisted to 290.0° ± 1.0°C (0.95 confidence interval based on eight tests). Fibrous crystals prepared from the same polymer in a different flow experiment persisted to the same temperature.[18] The birefringence of the spherulitic control sample, on the other hand, persisted to 267.0° ± 1.0°C (0.95 confidence interval based on six tests).

The results of the hot-stage experiments seem to firmly establish that the translucent segments possess a row-nucleated-type structure. Furthermore, the results show that fundamental similarities exist between the melting behavior of the translucent PET segments and that of various flow-crystallized materials prepared from polyethylene. Grubb et al. observed that oriented polyethylene samples which had been crystallized from both flowing melt and from stirred

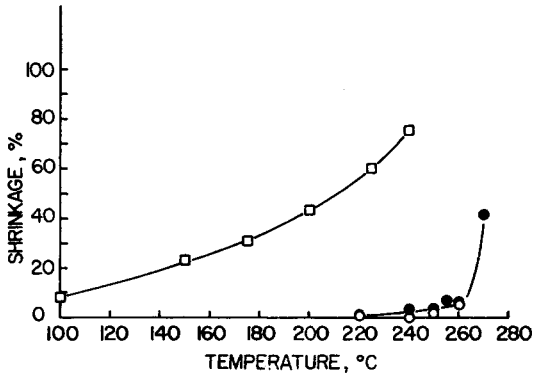

Fig. 18. Comparison of the shrinkage behavior of drawn PET yarn (data of Dumbleton[52]) (□) and translucent PET segments which were annealed in silicone oil for 1 min (○) and 1 hr (●): (○) 50–60 min extrusion time; (●) 5–15 min extrusion time.

solution exhibited a common melting characteristic: at a certain point in the temperature scan, the lamellar component of the sample melted but the fibrous component persisted. This melting characteristic was also, of course, exhibited by the translucent PET segments at about 266°C. Another point of similarity between the melting of flow-crystallized PET and the flow-crystallized polyethylenes was the exceptional thermal stability of the fibrous component. The birefringence of fibrils in samples prepared from both polymers persisted to temperatures well beyond the melting point of the lamellar component. The high thermal stability of the fibrous backbone in row-nucleated and shish-kebab morphologies prepared from polyethylene has been attributed to the presence of extended-chain material.[50,51] Presumably, the PET fibrils prepared in present work also possessed an extended-chain character.

Shrinkage Measurements

The shrinkage of segments prepared at 260°C was determined at several temperatures in the melting range of the polymer sample. The 1-hr shrinkage tests were performed solely on highly oriented, translucent segments which formed within the first 60 min of the extrusion experiment. To determine the effect of growth time in the capillary on the degree of shrinkage, we performed tests on segments which formed during short (5–15 min) and long (50–60 min) extrusion times.

The translucent segments exhibited remarkable dimensional stability. As Figure 18 shows, the shrinkage at 220°C was virtually negligible (1%–1.5%) for both sets of translucent segments. Yet even at 260°C, the shrinkage did not exceed 7%. Furthermore, at temperatures up to 260°C, the segments were still translucent after the shrinkage test, which also shows that the original morphology was not drastically affected by the severe annealing treatments. Consistent with the microscopic observation of initial melting at about 264°C, significant shrinkage became evident only at temperatures slightly above 260°C. Figure 18 also shows that the segments were preannealed during growth in the capillary, since the long-growth segments show lower shrinkage values than the short-growth segments at all test temperatures. However, the differences in

shrinkage between the two sets of samples over the range of test temperatures were small (0.5%–3.0%), which suggests that the dimensional stability of the translucent segments was not totally due to the effects of the preannealing treatment.

Figure 18 also compares the shrinkage behavior of the translucent segments with the shrinkage results of Dumbleton[52] for highly drawn years heated in silicone oil for 1 min. The comparison readily points out that the shrinkage of the drawn yarns was controlled by the noncrystalline phase of the initial structure, while the shrinkage of the translucent segments was limited by the stability of the crystalline phase. It has been generally recognized that the high shrinkage of drawn yarns of PET and nylon 66 results from the high mobility of oriented chains in the large noncrystalline phase.[52–54] However, the shape of the shrinkage curve for the translucent segments implies that significant shrinkage was possible only when the stable crystalline phase began to melt.

The exceptional dimensional stability of the translucent segments may be attributed to two factors. First, the low shrinkage may be largely due to the high thermal stability of the axially aligned fibrous backbones which formed during flow at the capillary entrance. Barham and Keller[55] have demonstrated that fibrous materials prepared by flow-induced crystallization generally exhibit a high resistance to shrinkage at temperatures just below the melting point. Under the same conditions, however, plastically deformed materials generally shrink drastically. The second factor which enhanced the inherent dimensional stability of the as-formed translucent morphology was the subsequent preannealing treatment in the capillary. During this unique treatment, the translucent segment was simultaneously constrained and annealed under high pressure. The size and perfection of both lamellar and fibrous components of the crystalline phase must have increased as a result.

CONCLUSIONS

A detailed study of the response of PET melts to high-pressure extrusion via the procedure of Southern and Porter has been completed. A wide range of techniques was used to examine the extrusion process and the properties of segments prepared at temperatures from 245° to 265°C.

The experiments established that polymer crystallizability exerts a powerful effect on the entire extrusion process. The results of the extrusion experiment with a given polymer are controlled in part by the high-pressure crystallization kinetics of the melt in the rheometer reservoir. With PET, the slowness of the phase transformation under constant pressure has some interesting consequences. Unlike the original experiments with polyethylene, with PET two mechanisms of segment formation may be detected. Initially, the converging flow of compliant melt in the conical entrance region of the die yields a highly oriented, translucent segment. However, as crystallization progresses in the rheometer reservoir, the formation mechanism of flow-induced crystallization eventually gives way to plastic deformation of solid polymer.

The experiments also established that converging flows may be used to prepare a unique fibrous morphology directly from PET melt. Besides being highly oriented, the translucent segments are highly crystalline and exhibit exceptional dimensional stability at temperatures up to 260°C. The evidence accumulated

in this study points strongly to a row-nucleated microstructure for the translucent segments; however, electron microscopy studies are needed for verification.

With the present procedure, an increase in extrusion temperature serves to increase the magnitude of the longitudinal velocity gradient at the capillary entrance. As a result, the crystalline orientation and melting point of the translucent segments also increase with increasing temperature. The structural properties of the segments improve significantly as the extrusion temperature is raised to 265°C, apparently because a higher concentration of nucleating fibrils are generated by the greatly enhanced velocity gradient at this temperature. The results raise the possibility that more intense extensional flows, when coupled with an improved extrusion technique, might be used to produce high-modulus row structures containing a large proportion of load-bearing fibrils and tie molecules. The intriguing possibility of forming the unique structure continuously by restricting the site of the phase transformation to the exit end of the die by imposing a temperature gradient on the die is now being studied.

The authors are grateful to Beaunit Corporation for use of the Instron capillary rheometer and to Camille Dreyfus Laboratory for use of x-ray equipment. We are indebted to Dr. Nicholas Morosoff and Mr. William Newton of Camille Dreyfus Laboratory for their generous help with the x-ray experimentation and interpretation. The PET sample used in this study was provided by the Goodyear Tire and Rubber Company. The technical assistance of Dr. Jack Hill of Goodyear is gratefully acknowledged. Special thanks are extended to Professor Waller George for useful discussions and suggestions. This research was generously funded by a grant from the Camille and Henry Dreyfus Foundation.

References

1. W. B. Black and J. Preston, *High-Modulus Wholly Aromatic Fibers,* Marcel Dekker, New York, 1973.
2. M. Bowman, U.S. Pat. 3,382,220 (May 7, 1968) Phillips Petroleum Company.
3. T. T. Wang, H. S. Chen, and T. K. Kwei, *Polym. Prepr., Am. Chem. Soc., Div. Polym. Chem.,* **11,** 939 (1970).
4. T. K. Kwei, T. T. Wang, and H. E. Bair, *J. Polym Sci. C,* **31,** 87 (1970).
5. J. H. Southern and R. S. Porter, *J. Macromol. Sci., Phys.,* **B4,** 541 (1970).
6. J. H. Southern and R. S. Porter, *J. Appl. Polym. Sci,* **14,** 2305 (1970).
7. K. Imada, T. Yamamoto, K. Shigematsu, and M. Takayanagi, *J. Mater. Sci.,* **6,** 537 (1971).
8. D. Krueger and G. S. Y. Yeh, *J. Appl. Phys.,* **43,** 4339 (1972).
9. M. R. Mackley and A. Keller, *Polymer,* **14,** 16 (1973).
10. To Imperial Chemical Industries, Belg. Pat. 813,398 (Oct. 7, 1974).
11. A. Siegmann, U.S. Pat. 3,846,377 (Nov. 5, 1974) Allied Chemical Corporation.
12. C. R. Desper, J. H. Southern, R. D. Ulrich, and R. S. Porter, *J. Appl. Phys.,* **41,** 4284 (1974).
13. R. G. Crystal and J. H. Southern, *J. Polym. Sci. A-2,* **9,** 1641 (1971).
14. N. E. Weeks, S. Mori, and R. S. Porter, *J. Polym. Sci., Polym. Phys. Ed.,* **13,** 2031 (1975).
15. N. E. Weeks and R. S. Porter, *J. Polym. Sci., Polym. Phys. Ed.,* **13,** 2049 (1975).
16. N. E. Weeks and R. S. Porter, *J. Polym. Sci., Polym. Phys. Ed.,* **12,** 635 (1974).
17. N. J. Capiati and R. S. Porter, *J. Polym. Sci., Polym. Phys. Ed.,* **13,** 1177 (1975).
18. P. D. Griswold and J. A. Cuculo, to appear.
19. W. H. Cobbs and R. L. Burton, *J. Polym. Sci.,* **10,** 275 (1953).
20. A. Keller, G. R. Lester, and L. B. Morgan, *Proc. R. Soc. (London),* **A247,** 1 (1954).
21. H. P. Schreiber, *Polym. Eng. Sci.,* **6,** 317 (1966).
22. R. L. Ballman, *J. Appl. Polym. Sci.,* **7,** S27 (1963).
23. I. Marshall and A. Todd, *Trans. Faraday Soc.,* **49,** 67 (1953).
24. R. C. Wampler and D. R. Gregory, *J. Appl. Polym. Sci.,* **16,** 3253 (1972).
25. T. F. Ballenger and J. L. White, *J. Appl. Polym. Sci.,* **15,** 1949 (1971).
26. R. G. Scott, *ASTM Bull.,* **257,** 121 (1959).

27. K. Imada and M. Takayanagi, *Int. J. Polym. Sci.*, **2,** 89 (1973).
28. J. H. Southern, N. E. Weeks, R. S. Porter, and R. G. Crystal, *Makromol. Chem.*, **162,** 19 (1972).
29. W. J. Dulmage and A. L. Geddes, *J. Polym. Sci.*, **31,** 499 (1958).
30. C. J. Heffelfinger and R. L. Burton, *J. Polym. Sci.*, **47,** 289 (1960).
31. I. Kuriyama and K. Shirakashi, *Sen-i-Gakkaishi,* **20,** 356 (1964).
32. L. Mandelkern, *Crystallization of Polymers,* McGraw-Hill, New York, 1964, pp. 215–290.
33. S. Matsuoka and B. Maxwell, *J. Polym. Sci.*, **32,** 131 (1958).
34. A. Keller and M. H. Machin, *J. Macromol. Sci., Phys.*, **B1,** 41 (1967).
35. J. E. Spruiell, D. E. McCord, and R. A. Beuerlein, *Trans. Soc. Rheol.*, **16,** 535 (1972).
36. L. E. Alexander, *X-Ray Diffraction Methods in Polymer Science,* Wiley, New York, 1969, p. 334.
37. A. Peterlin, *Text. Res. J.*, **42,** 20 (1972).
38. H. A. Stuart, *Ann. New York Acad. Sci.*, **83,** 3 (1959).
39. J. P. Sibilia, P. J. Harget, and G. A. Tirpak, *Polym. Prepr., Am. Chem. Soc., Div. Polym. Chem.*, **15,** 660 (1974).
40. F. J. Baltá-Calleja and A. Peterlin, *J. Macromol. Sci., Phys.*, **B4,** 519 (1970).
41. W. O. Statton, *J. Polym. Sci.*, **17,** 143 (1959).
42. P. J. Holdsworth and A. Turner-Jones, *Polymer,* **12,** 195 (1971).
43. R. C. Roberts, *Polymer,* **10,** 117 (1969).
44. D. L. Nealy, T. G. Davis, and C. J. Kibler, *J. Polym. Sci. A-2,* **8,** 2141 (1970).
45. G. E. Sweet and J. P. Bell, *J. Polym. Sci. A-2,* **10,** 1273 (1972).
46. G. Miller, *Thermochim. Acta,* **8,** 129 (1974).
47. A. Miyagi and B. Wunderlich, *J. Polym. Sci. A-2,* **10,** 1401 (1972).
48. A. Miyagi and B. Wunderlich, *J. Polym. Sci., Polym. Phys. Ed.*, **10,** 2073 (1972).
49. D. T. Grubb, J. A. Odell, and A. Keller, *J. Mater. Sci.*, **10,** 1510 (1975).
50. M. J. Hill and A. Keller, *J. Macromol. Sci., Phys.*, **B5,** 591 (1971).
51. A. Keller and F. M. Willmouth, *J. Macromol. Sci., Phys.*, **B6,** 493 (1972).
52. J. H. Dumbleton, *J. Polym. Sci. A-2,* **7,** 667 (1969).
53. P. F. Dismore and W. O. Statton, *J. Polym. Sci. C,* **13,** 133 (1966).
54. R. J. Samuels, *J. Polym. Sci. A-2,* **10,** 781 (1972).
55. P. Barham and A. Keller, *J. Polym. Sci., Polym. Lett. Ed.*, **13,** 197 (1975).

Received September 30, 1976
Revised November 17, 1976